Dual-Targeting Upconversion Nanoprobes across the Blood–Brain Barrier for Magnetic Resonance/Fluorescence Imaging of Intracranial Glioblastoma

Dalong Ni,[†] Jiawen Zhang,[‡] Wenbo Bu,[†,*] Huaiyong Xing,[†] Fang Han,[‡] Qingfeng Xiao,[†] Zhenwei Yao,[‡] Feng Chen,[†] Qianjun He,[†] Jianan Liu,[†] Shengjian Zhang,[§] Wenpei Fan,[†] Liangping Zhou,[§] Weijun Peng,[§] and Jianlin Shi[†,*]

[†]State Key Laboratory of High Performance Ceramics and Superfine Microstructures, Shanghai Institute of Ceramics, Chinese Academy of Sciences, Shanghai 200050, China, [‡]Department of Radiology, Huashan Hospital, Fudan University, Shanghai 200040, China, and [§]Department of Radiology, Shanghai Cancer Hospital, Fudan University, Shanghai 200032, China

ABSTRACT Surgical resection, one of the main clinical treatments of intracranial glioblastoma, bears the potential risk of incomplete excision due to the inherent infiltrative character of the glioblastoma. To maximize the accuracy of surgical resection, the magnetic resonance (MR) and fluorescence imaging are widely used for the tumor preoperative diagnosis and intraoperative positioning. However, present commercial MR contrast agents and fluorescent dyes can only function for single mode of imaging and are subject to poor blood–brain barrier (BBB) permeability and nontargeting-specificity, resulting in the apparent risks of inefficient diagnosis and resection of glioblastoma. Considering the unique MR/upconversion luminescence (UCL) bimodal imaging feature of upconversion nanoparticles (UCNPs), herein, we have developed a dual-targeting nanoprobe (ANG/PEG-UCNPs) to cross the BBB, target the glioblastoma, and then function as a simultaneous MR/NIR-to-NIR UCL bimodal imaging agent, which showed a much enhanced imaging performance in comparison with the clinically used single MRI contrast (Gd-DTPA) and fluorescent dye (5-ALA). Moreover, their biocompatibility, especially to brains, was systematically assessed by the histological/hematological examination, indicating a negligible *in vivo* toxicity. As a proof-of-concept, the ANG/PEG-UCNPs hold the great potential in MR diagnosis and fluorescence positioning of glioblastoma for the efficient tumor surgery.

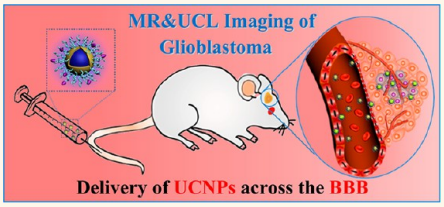

KEYWORDS: upconversion nanoparticles · blood-brain barrier · glioblastoma · contrast agent · bimodal imaging

Glioblastoma, the most aggressive and common intracranial tumor, is considered as the major cause of death from central nervous system (CNS) cancers.[1] The median survival periods for these patients remain less than 15 months even after surgical intervention followed by chemo-radiation therapy.[2,3] Surgical resection, one of the main clinical treatment approaches for intracranial glioblastoma, frequently suffers from the incomplete excision due to the heterogeneous and infiltrative character of glioblastoma and thus fails to completely eradicate tumor,[4,5] leading to inevitable tumor recurrence within 6–12 months postsurgery.[6] To guide glioblastoma excision before and during surgical resection, a tumor-targeted imaging contrast agent (CA), which is capable of both the tumor preoperative diagnosis and intraoperative positioning of lesion areas, is urgently required to substantially improve the accuracy of surgical resection with the least damage to CNS.

Currently, magnetic resonance imaging (MRI) as a common diagnostic method has been used to diagnose the brain tumor preoperatively.[7] Gadolinium (Gd)-based MR CAs such as Magnevist (Gd-DTPA) are being widely used to delineate the glioblastoma macroscopical margins in clinics.[8] However, the blood–brain barrier (BBB), which is one of the most exclusive biological barriers,[9] limits the intracephalic uptake of

* Address correspondence to wbbu@mail.sic.ac.cn, jlshi@mail.sic.ac.cn.

Received for review August 7, 2013 and accepted January 7, 2014.

Published online January 07, 2014
10.1021/nn406197c

these CAs.[10,11] Therefore, more than 10% glioblastoma and 30% anaplastic astrocytomas fail to display any MR signal enhancement due to the uncompromised BBB.[12] Moreover, the lack of tumor specificity and the rapid renal clearance of these CAs further deteriorate their contrast efficacies and impede their effective application in accurate glioblastoma diagnosis.[13] Compared with these small molecular CAs, the multifunctional nanoprobes with unique nanometer size and advantageous surface modifications possess long blood circulation half-lives, consequently exhibiting the enhanced imaging contrast.[14] Furthermore, with specific antibodies or peptides conjugated on the surface, these nanoprobes could cross the BBB by receptor-mediated transcytosis (RMT),[15−17] absorptive-mediated transcytosis (AMT),[18,19] or both of them.[20] Recently, the report from Gao's group on the BBB transport of MR CAs suggested that RMT was an effective approach to mediate nanoprobes across the BBB, but unfortunately, this research was only confined to healthy brain MRI.[15] The preoperative MRI glioblastoma diagnosis by using CAs, even though capable of crossing BBB by RMT, still suffers from the lack of tumor specificity and remains therefore a great challenge.

In addition to the preoperative MRI scanning, the fluorescence-guided resection was also used for the visual contrast of glioblastoma to assist the excision of this aggressive tumor during surgery.[21−26] One clinically used method is to use five-aminolevulinic acid (5-ALA), which can be taken up by glioblastoma cells and converted into fluorescent protoporphyrin IX (PpIX) therein, and then emit red fluorescence under blue light illumination.[25] However, the blue excitation light of PpIX, unfortunately, is confronted with the low tissue penetration depth and the inevitable autofluorescence. Moreover, the 5-ALA-converted PpIX suffers from poor photostability and heavy photobleaching.[26] In contrast, upconversion nanoparticles (UCNPs) can be excited by 980 nm near-infrared (NIR) light in the "optical transmission window" of biological tissues (750−1000 nm) and emit strong visible-to-NIR luminescence signal with photostability, nonblinking fluorescence, high tissue penetration and reduced photodamage.[27−36] Furthermore, Gd-doped UCNPs have been recognized as the promising MR/upconversion-luminescence (UCL) bimodal imaging nanoprobes.[36−41] These nanoprobes have been demonstrated to be feasible for the MR/UCL imaging of subcutaneously xeno-transplanted U87MG tumors.[42,43] However, the penetration of the Gd-doped UCNPs across the BBB and the application in intracranial glioblastoma imaging, which are much more challenging and rewarding in glioblastoma surgery, have not been addressed so far.

In this study, a kind of bimodal imaging Gd-doped UCNPs has been first developed for the dual MR and NIR-to-NIR UCL imaging of glioblastoma. Angiopep-2 (ANG, TFFYGGSRGKRNNFKTEEY), here used as a dual-targeting ligand, has been confirmed to be able to specially bind to the low density lipoprotein receptor related protein (LRP), which is overexpressed on both BBB and glioblastoma cells.[44−46] To the best of our knowledge, it is the first time to couple ANG with PEGylated UCNPs for constructing the UCNPs-based dual-targeting imaging nanoprobes (ANG/PEG-UCNPs). Systematic *in vitro* and *in vivo* MR and NIR-to-NIR UCL imagings of intracranial glioblastoma were performed to evaluate their BBB-crossing and tumor specific targeting efficacy. We also demonstrate that the ANG/PEG-UCNPs show a much enhanced bimodal imaging performance as compared to the clinically used single-mode imaging contrast Gd-DTPA (for MRI) and 5-ALA (for fluorescence imaging). This bimodal imaging contrast agent, with the negligible *in vivo* toxicity as confirmed by the histological/hematological examination, holds a great potential in future MR diagnosis and fluorescence positioning for the efficient glioblastoma surgery.

RESULTS AND DISSCUSSION

Synthesis and Characterizations of ANG-PEG-UCNPs. Scheme 1a illustrates the structure of ANG/PEG-UCNPs. The synthesis includes three typical steps. First, the monodisperse UCNPs ($NaYF_4$:20%Yb/2%Tm/15%Gd@$NaGdF_4$) capped with oleic acid (OA) ligands were prepared using our reported method.[41,47] The introduction of gadolinium ions significantly promote the formation of small-sized $NaYF_4$:Yb/Tm/Gd core. Meanwhile the coated ultrathin $NaGdF_4$ shell can greatly enhance the upconversion luminescence intensity and facilitate its utility as a MRI CA.[41,47] Subsequently, the hydrophobic UCNPs were transferred into aqueous phase by using hydrochloric acid (HCl) to eliminate the OA,[48] and then were capped with amine-poly(ethylene glycol)-thiol (NH_2-PEG_{5k}-SH) through the strong thiol-metal attraction forming PEG-UCNPs.[49] Finally, the as-obtained PEG-UCNPs were further decorated with ANG through the conjugation between the amino groups on PEG-UCNPs and the carboxyl groups of ANG,[44] resulting in the ANG/PEG-UCNPs nanocomposites.

As shown in the TEM images (Figure 1a,b, and Figures S1a, S2a), $NaYF_4$:Yb/Tm/Gd and $NaYF_4$:Yb/Tm/Gd@$NaGdF_4$ exhibit uniform spherical nanoparticles and well-defined size distributions with average particle sizes of 17.2 ± 0.5 and 19.3 ± 0.7 nm (over 300 nanoparticles were estimated using low-magnification TEM images), respectively. The thickness of the coated $NaGdF_4$ shell is roughly estimated to be around 1 nm. Energy-dispersive X-ray (EDX) spectrum (Figures S1 and S2) demonstrated the existence of all the expected basic chemical elements (Na, Y, F, Yb, Tm and Gd), and the powder X-ray diffraction (XRD, Figure S3) spectra displayed their pure hexagonal phase structure with high crystallinity and no visible cubic phase.

No significant changes in the morphology and composition of UCNPs were observed after the surface

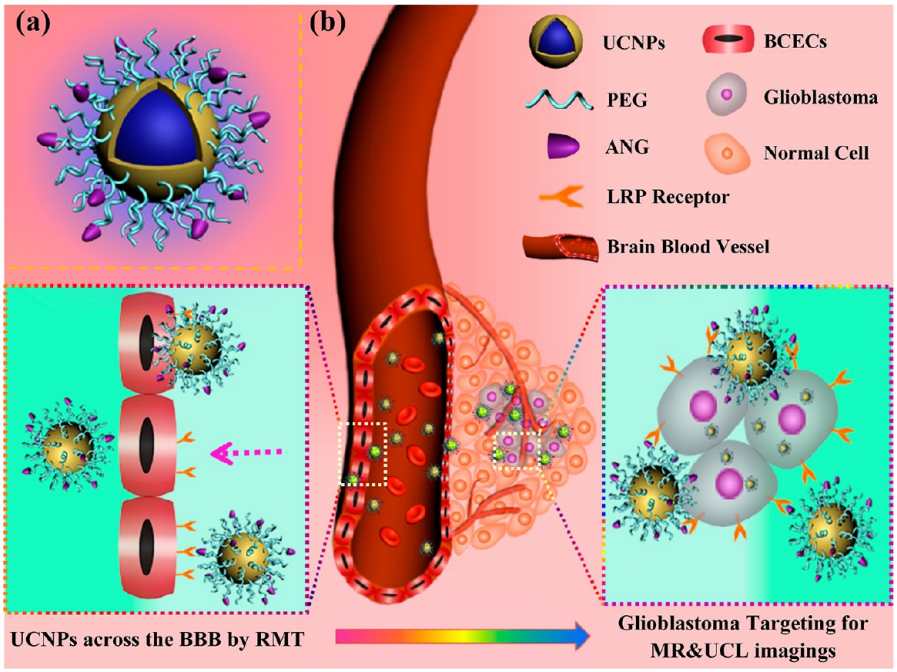

Scheme 1. (a) Design of the dual-targeting ANG/PEG-UCNPs. (b) Schematic diagram of the ANG/PEG-UCNPs as the dual-targeting system to cross the BBB and target the glioblastoma *via* LRP mediated endocytosis, enabling MR and UCL imaging of intracranial glioblastoma.

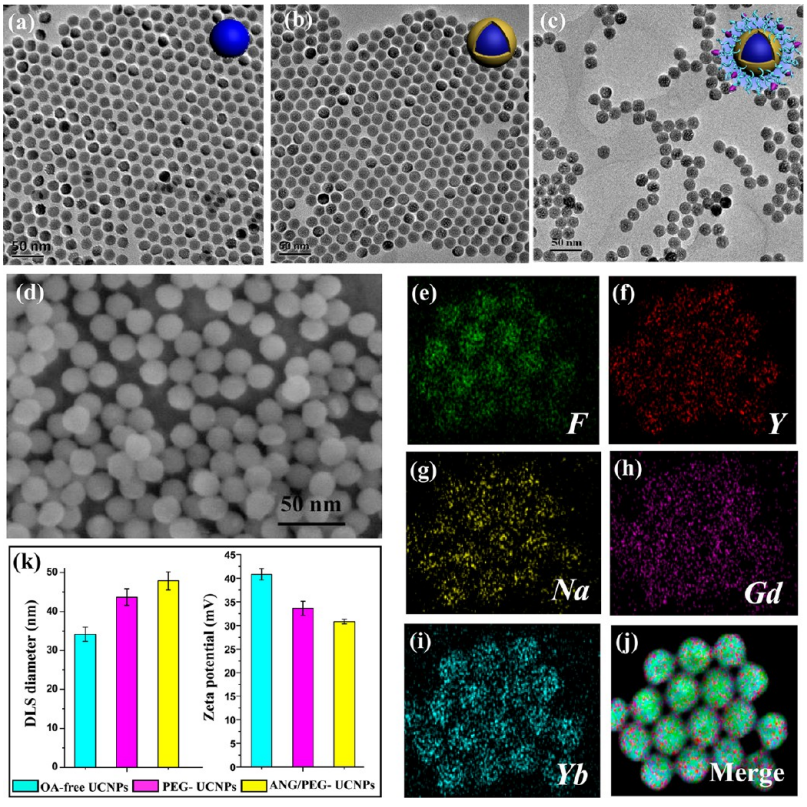

Figure 1. The synthesis and characterization of ANG/PEG-UCNPs: TEM images of (a) core ($NaYF_4$:Yb/Tm/Gd), (b) UCNPs ($NaYF_4$:Yb/Tm/Gd@$NaGdF_4$), and (c) ANG/PEG-UCNPs; (d) SEM image of ANG/PEG-UCNPs; (e–j) element mappings (F, Y, Na, Gd and Yb) of ANG/PEG-UCNP; (k) Dynamic light scattering (DLS) sizes (left) and zeta-potentials (right) of OA-free UCNPs, PEG-UCNPs, and ANG/PEG-UCNPs.

modifications, as evidenced by TEM imaging shown in Figure 1c, SEM imaging in Figure 1d and element mappings (F, Y, Na, Gd and Yb) in Figure 1e–j. The molar percentage of each rare earth element in

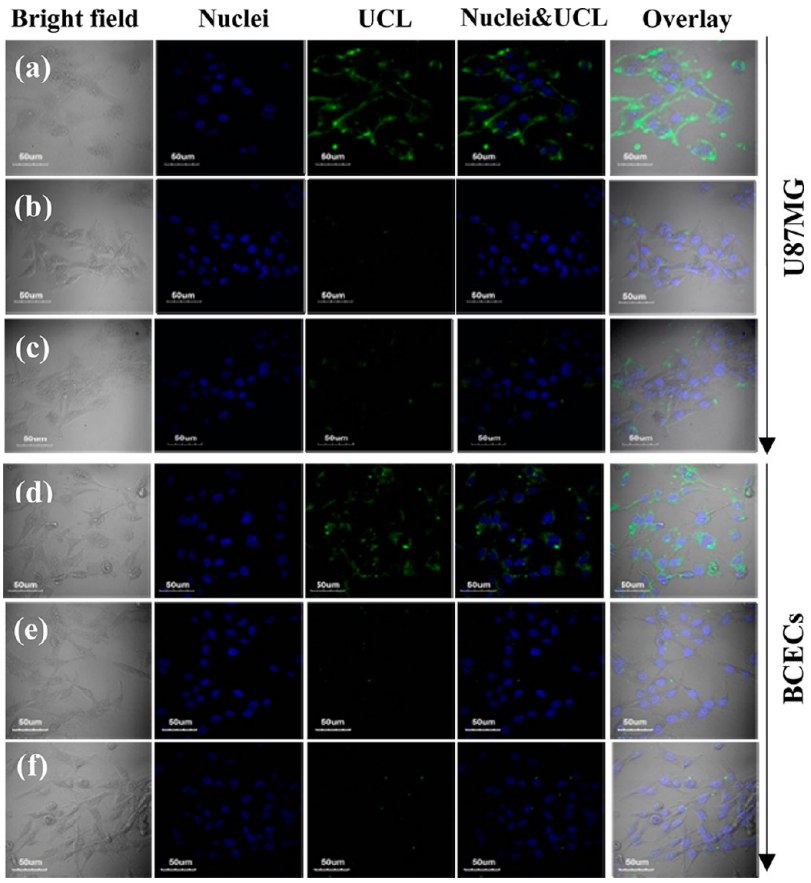

Figure 2. Representative confocal UCL images of U87MG and BCECs incubated with (a and d) ANG/PEG-UCNPs, (b and e) PEG-UCNPs, or (c and f) ANG/PEG-UCNPs under the free ANG blocking. Concentrations of all samples were fixed at 300 μg/mL.

ANG/PEG-UCNPs was measured to be 60.9% (Y), 20.5% (Yb), 1.9% (Tm), and 16.7% (Gd), by the inductively coupled plasma optical emission spectrometry (ICP-OES) (Table S1). The variations associated with the characteristic functional groups in Fourier transform infrared (FT-IR) spectra verify the successful OA elimination, PEG coating and ANG modification (Figure S4). In addition, S and O elements were presented in ANG/PEG-UCNPs (Figure S5) in addition to the basic chemical elements of UCNPs (Figure S2), implying the successful conjugations of the PEG chains and ANG molecules, which were further confirmed by both the dynamic light scattering (DLS) and zeta-potential measurements as show in Figure 1k and Table S2. The diameters of UCNPs based on DLS measurements after each step of surface modification become a little larger to varied extents because of the presence of hydrated layers, PEG chains,[50] and ANG molecules. After removing the oleic acid (OA) ligands, the bare NPs showed a positive zeta-potential (+40.8 ± 1.2 mV) due to the existence of rare earth ions (Y^{3+}, Tm^{3+}, Gd^{3+}, and Yb^{3+}) on the surface. Then, the negative shift in the zeta-potential from OA-free UCNPs to PEG-UCNPs (+33.6 ± 1.5 mV) is caused by the formation of a PEG layer which shields the surface charge of the UCNPs. And after the conjugation of the neutral Angiope-2, the final surface charge and DLS diameter of ANG/PEG-UCNPs were found to be 30.8 ± 0.5 mV and 47.9 ± 2.2 nm, respectively. The color reactions based on the Bradford method demonstrate the successful ANG modification and the removal of free ANG (Figure S6a−d). Moreover, the control experiments using MeO-PEG_{5k}-SH confirmed that the ANG was covalently coupled to the PEG (Figure S6e,f). The amount of ANG on the surface of each nanoparticle was calculated as ~76 ANG molecules per UCNP particle according to the results of Bradford method (Table S2).

The luminescence spectrum of ANG/PEG-UCNPs under the NIR laser (λ = 980 nm) excitation exhibits two weak blue bands (448 nm, $^1D_2 \rightarrow {}^3F_4$; 476 nm, $^1G_4 \rightarrow {}^3H_6$) and a strong NIR band (800 nm, $^3H_4 \rightarrow {}^3H_6$) (Figure S7). As shown in Figure S8, its blue emission is highly dependent on the initial concentration of the NPs and the power of the laser. Moreover, to demonstrate the relatively high tissue penetration of NIR excitation, the PpIX, which is the final transformational product of 5-ALA during the clinical brain tumor surgery, was used as a control. The results show that PpIX can emit red fluorescence under the 470 nm excitation, but no visible emission can be observed under the 1 mm-thick pork obstruction. Noticeably, ANG/PEG-UCNPs still emit strong blue light at 980 nm excitation even under a 5 mm-thick pork obstruction

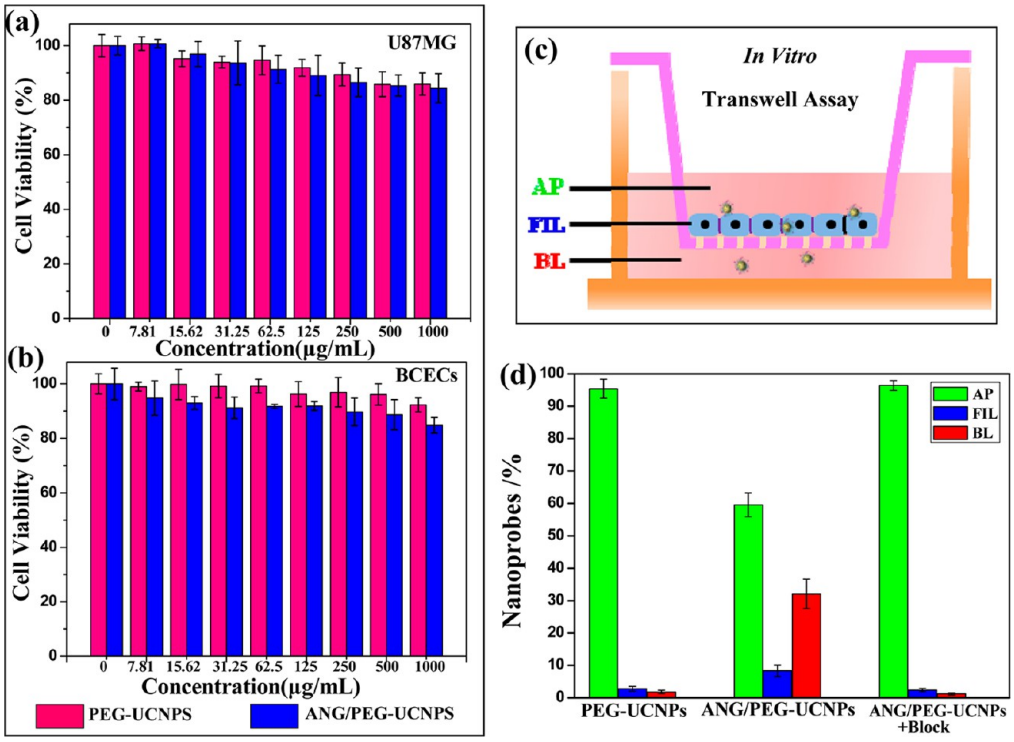

Figure 3. *In vitro* **cell viabilities of (a) U87MG and (b) BCECs incubated with NPs for 24 h. (c) Schematic overview of the BCECs transwell assay for NPs to cross the BBB** *in vitro***. (d) The relative transcytosis amount of PEG-UCNPs, ANG/PEG-UCNPs, and ANG/PEG-UCNPs under the blocking of free ANG** *in vitro***.**

owing to the relatively high tissue penetration of NIR. (Figure S9), which is consistent well with the reported results.[30,35]

The MRI of ANG/PEG-UCNPs acquired on a 3.0 T MR scanner reveals the concentration-dependent brightening effect (Figure S7b), giving a specific relaxivity r_1 value of 2.28 mM^{-1} s^{-1} (Figure S7c,d). According to the previously reported "negative-lattice shield effect" (n-LSE), the longitudinal relaxivity of Gd ions in shortening T_1-weighted relaxation time of water proton is mainly contributed by the surface Gd ions in nanoparticles.[41,51,52] Therefore, compared with $NaYF_4$:Yb/Er/Gd (r_1 = 0.14 mM^{-1} s^{-1}),[39] the specific relaxivity r_1 value of ANG/PEG-UCNPs was remarkably enhanced by about 15-fold as expected, owing to the higher surface Gd ion concentration compared to the particles without the layer. However, such a r_1 value is still smaller than that of ultrasmall-NaGd[74.5%]F_4:Yb/Tm (r_1 = 3.37 mM^{-1} s^{-1} at 1.4 T)[53] recently reported by Capobianco *et al.*, as these ultrasmall NPs (<5 nm in diameter) with high specific surface ratios could maximize dipole−dipole interactions between Gd ions and hydrogen protons but minimize the fluorescence performance as compared to the hexagonal $NaYF_4$-host lattice of the present ANG/PEG-UCNPs (~20 nm).[29,54,55] Through PEGylation, ANG/PEG-UCNPs acquired a long *in vivo* blood circulation half-life of up to 72.4 min (Figure S10a), which was much longer than that of the clinically used Gd-DTPA (about 12.7 min, Figure S10b). Compared with the rapid renal clearance of Gd-DTPA, the long circulation lifetime of ANG/PEG-UCNPs benefits the both targeting and imaging because theses targeting agents could avoid the rapid uptake by the reticuloendothelial system (RES) and could therefore accumulate in the targeted tissues.

Enhanced Cellular Uptake of ANG/PEG-UCNPs. We first studied the *in vitro* cytotoxicity against U87MG and BCECs by a typical MTT assay (Figure 3a,c). It is shown that above 85% of the cells can survive even after the co-incubation with an extremely high concentration (1000 μg/mL) of ANG/PEG-UCNPs or PEG-UCNPs for 24 h, demonstrating the low cytotoxicity of these NPs *in vitro*. Confocal microscopic imaging was then used to confirm the enhanced uptake of the ANG/PEG-UCNPs *in vitro*. As shown in Figure 2, maximum upconversion fluorescence under 980 nm excitation can be observed around the nucleus of the U87MG and BCECs after their incubation with ANG/PEG-UCNPs (Figure 2a,d), which implies that ANG/PEG-UCNPs have been uptaken by cells into the cytoplasm. In contrast, when U87MG and BCECs were incubated with PEG-UCNPs alone, only faint fluorescence signals could be observed (Figure 2b,e). The significantly higher uptakes of ANG/PEG-UCNPs than PEG-UCNPs by U87MG and BCECs can be clearly attributed to the targeting interaction between ANG and LRP receptor, which was further demonstrated by a typical blocking assay. Only weak fluorescence was observed in both U87MG and BCECs incubated with the ANG/PEG-UCNPs under high-dose ANG blocking (Figure 2c,f). On the basis of

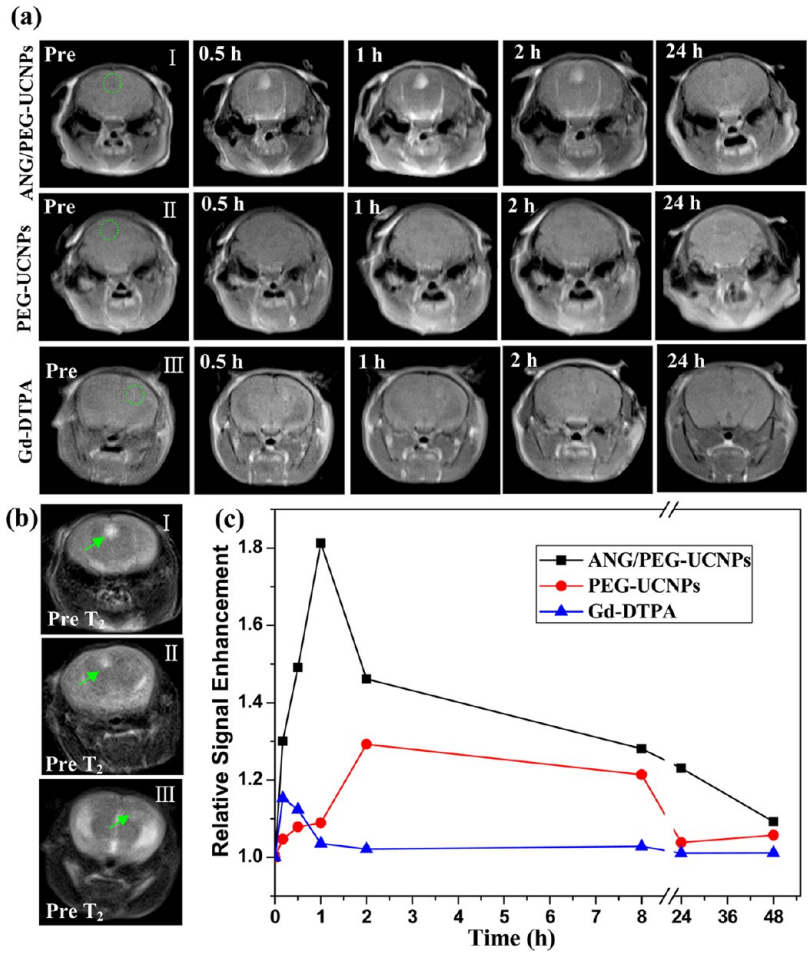

Figure 4. *In vivo* **MRI and the quantitive signal enhancements in glioblastoma-bearing mice before and at various time points after the intravenous injections. (a) T_1-weighted MR images of ANG/PEG-UCNPs, PEG-UCNPs and Gd-DTPA. (b) T_2-weighted MRI was performed to confirm the location of the glioblastoma (cyanic arrow). (c) Quantitative analysis results of SI in the T_1-weighted MR images (ROI).**

the above results, it can be concluded that the ANG/PEG-UCNPs can significantly enhance uptake both in U87MG and BCECs by their specific binding to LRP receptor.

Transport across the BBB *in Vitro* and *in Vivo*. The *in vitro* BBB-targeting efficacy of ANG/PEG-UCNPs was measured by using transwell filters seeded with a compact BCECs monolayer (Figure 3c) according to the previously reported method.[45] To evaluate the BBB-crossing efficacy of ANG/PEG-UCNPs, the Gd contents on the apical side (AP), cellular monolayer (FIL), and basolateral side (BA) were analyzed by ICP-OES. The integrity of the BCECs monolayer *in vitro* was monitored by Transendothelial Electrical Resistance (TEER) value during the experiments, which was typically above 200 Ω cm^2. Figure 3d reveals that ANG/PEG-UCNPs possess the most prominent transport capability compared with other groups. Remarkably, 32.1 $\pm$ 4.5% of the targeting NPs were found on the basolateral side, but only 1.8 $\pm$ 0.5% of nontargeting PEG-UCNPs could be detected under the same condition. In addition to the significant increase of transport ratio across the BBB, the targeting ANG/PEG-UCNPs showed an enhanced affinity with the cells (Figure 3d, FIL). About 8.3 $\pm$ 1.8% of the total added targeting NPs remained cell-uptaken, three times as high as that of the nontargeting PEG-UCNPs, which indicated that the ANG had played a specific role in mediating the BBB-crossing transcytosis of the NPs. This receptor-mediated transcytosis (RMT) was further demonstrated by a blocking study. Excess free ANG was preincubated in the apical medium to competitively bind to LRP receptors on the *in vitro* BBB model, which resulted in significantly reduced transport ratio of ANG/PEG-UCNPs to the level of PEG-UCNPs (Figure 3d). Together, these data strongly demonstrate the critical role of RMT in crossing the BBB of ANG/PEG-UCNPs.

To further demonstrate the capability of ANG/PEG-UCNPs in transporting across the BBB, the *in vivo* brain MRI of normal mice was adopted to monitor the variations of T_1-weight MR signal intensity (SI) after the intravenous injection of ANG/PEG-UCNPs. To facilitate the quantitative analysis of the contrast enhancement, the regions of interest (ROI) were localized in

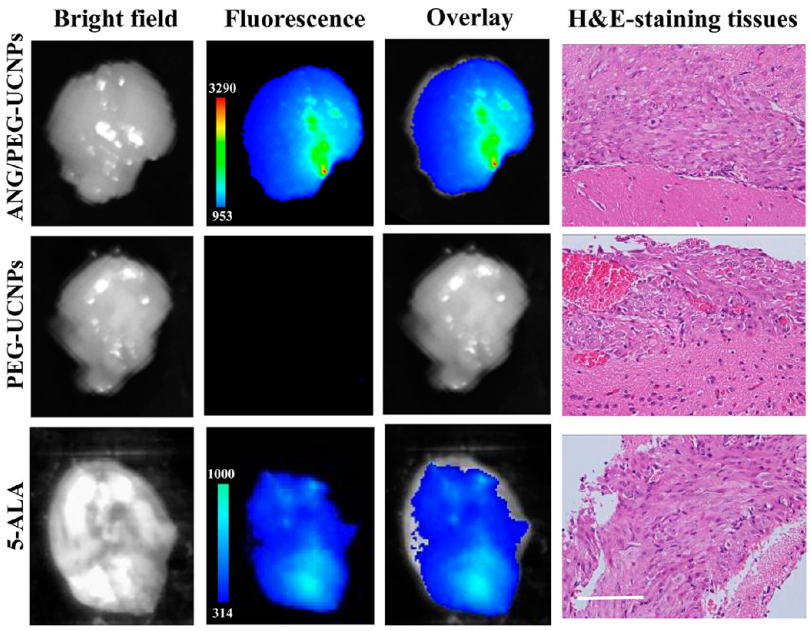

Figure 5. *Ex vivo* **fluorescent images of glioblastoma-bearing brain in 1 h after the intravenous injection with ANG/PEG-UCNPs, PEG-UCNPs (excitation, 980 nm; emission, 800 nm) and 5-ALA (excitation, 470 nm; emission, 650 nm). All imaging experiments were performed under the same condition. H&E-staining of the tumor tissues from glioblastoma-bearing mice brain was used to demonstrate the existence of glionblastoma. Scale bar: 100 μm.**

each MR image with fixed size and matching position. The results show that the SI gradually increases and reaches a large enhancement by about 30.9% in ~1 h postinjection (Figure S10c), suggesting that ANG/PEG-UCNPs could transport across the intact BBB *in vivo*. In contrast, the clinically used Gd-DTPA suffered from a short imaging time (about 10 min) with a limited SI enhancement of about 12.7% due to the BBB. These results clearly demonstrate the advantage of ANG/PEG-UCNPs in crossing the BBB, which leads to a much enhanced brain MRI efficacy than clinical Gd-DTPA.

MRI of Intracranial Glioblastoma *in Vivo*. The intracranial glioblastoma targeting capability by the ANG-mediated transport of the UCNPs across the BBB was investigated by using glioblastoma-bearing mice as a model (Scheme 1b). Prior to injection of NPs, T_2-weighted MRI was performed to confirm the location of the glioblastoma (Figure 4b). The time points of 10 min, 0.5, 1, 2, 8, 24, and 48 h postinjection (p.i.) were chosen for T_1-weighted MRI after the intravenous injection of ANG/PEG-UCNPs or PEG-UCNPs. The brain slices that contain the glioblastoma are shown in Figure 4a and Figure S11. Quantitative data obtained from ROI analysis of the MR images are shown in Figure 4c. In addition, the clinical Gd-DTPA was also used for direct comparison.

Figure 4a showed that T_1-weighted MR contrast of the glioblastoma in the targeting group was significantly enhanced and the tumor boundary was also much more clearly delineated as compared to the nontargeting group and the Gd-DTPA group under the same experimental conditions. The tumor-targeting behaviors of the ANG/PEG-UCNPs could be more clearly observed from the quantitative analysis on the SI of tumor area, as shown in Figure 4c. In general, the average SI of the tumor region began to increase immediately after the injection of ANG/PEG-UCNPs, reaching a maximal ~81.3% enhancement in ~1 h p.i. due to their highly efficient tumor targeting after crossing the BBB. The MR contrast maintains significant for a long time period (more than 2 h). Comparatively, the PEG-UCNPs administration shows a limited maximal contrast enhancement by about 29.2% in ~2 h p.i. due to the enhanced permeability and retention (EPR) effect (Figure 4c). In contrast, the enhancements of SI of the Gd-DTPA group was rather weak, with a maximal enhancement being about 15.2% in ~10 min p.i., and after that, the SI enhancement began to decrease due to rapid renal clearance of Gd-DTPA from the blood pool. Overall, the MR images and the corresponding brain tumor SI enhancement data evidence the significant LRP receptor specificity of ANG/PEG-UCNPs *in vivo*, validating that the ANG/PEG-UCNPs indeed possesses unambiguous advantages over the clinical Gd-DTPA in crossing the BBB and targeting the brain tumor for MRI.

NIR-to-NIR Fluorescence Imaging of Intracranial Glioblastoma *ex Vivo*. Encouraged by the exciting targeting efficacy of ANG/PEG-UCNPs in MRI modality, the NIR-to-NIR UCL imaging experiments were then performed on intracranial glioblastoma-bearing mice by the intravenous administrations of ANG/PEG-UCNPs and PEG-UCNPs. In addition, the clinical fluorescent dye 5-ALA was also used for direct comparison. After sacrificing the mice, the *ex vivo* fluorescent imagings of dissected organs were performed. The signal is much stronger in liver than that in spleen, while negligible signals were observable in other organs such as heart, lung and kidney for both

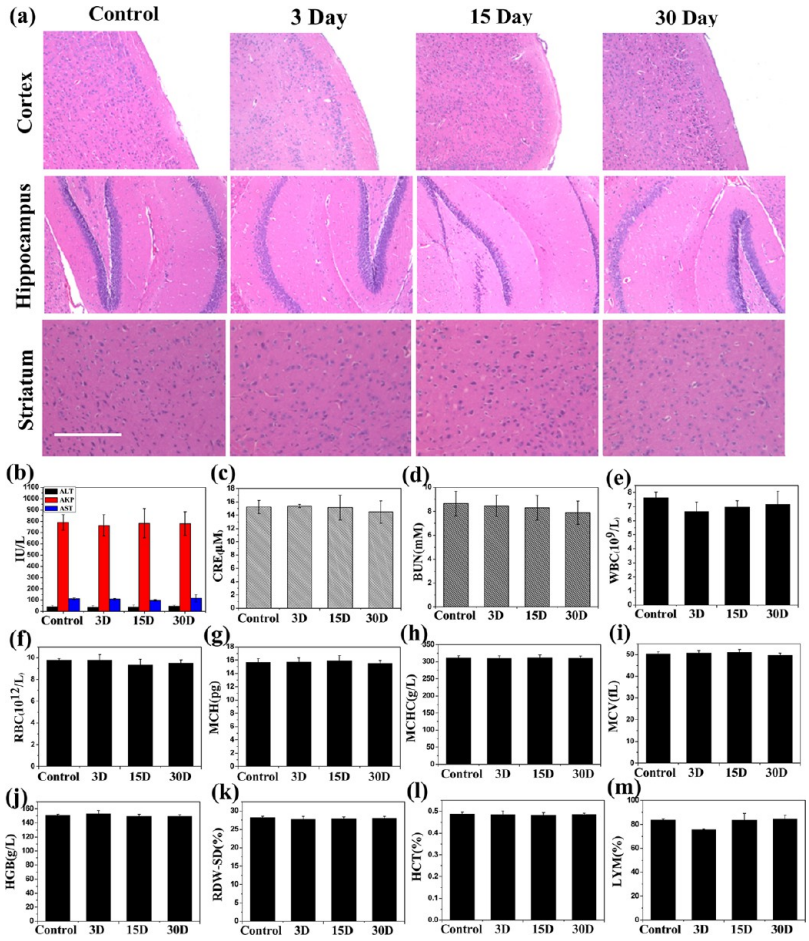

Figure 6. Toxicity studies of NPs *in vivo*. (a) H&E-stained tissues from mice brain to monitor the histological changes in cortex, hippocampus and striatum of brain after the intravenous injection of ANG/PEG-UCNPs (15 mg Y/kg) at different time points or receiving no injection as control. Scale bar: 200 μm. (b−m) Blood biochemistry data obtained from mice after the intravenous injection of ANG/PEG-UCNPs (n = 5, dose = 15 mg Y/kg) at various time points or receiving no injection as control.

targeting and nontargeting groups (Figure S12a,b). For 5-ALA group, the fluorescence can be observed in liver and kidney (Figure S12c). Moreover, the enhanced UCL signal from the brain tumor and the weak UCL signal from the other normal tissue in brain can be clearly observed in the targeting group (Figure 5), whereas no signal can be observed from the brain tumor in the nontargeting group. Comparatively, no signal intensity enhancement in brain tumor but only gross fluorescence signal in the whole brain can be observed in the 5-ALA group even after injection with a high dose of 5-ALA (90 mg/kg), as shown in Figure 5. After the fluorescence imagings, the mice brains were frozen, and the H&E-stained tumor sections from mice brain show the existence of brain tumor (Figure 5). Such a glioblastoma-targeted UCL imaging, with its preponderance over the clinical 5-ALA, can be possibly used for fluorescence-guided resection during the surgery of the infiltrative glioblastoma to improve the effectiveness and accuracy of surgical resection in combination with MRI.

To further confirm the targeting specificity of ANG/PEG-UCNPs to the LRP receptor, the *in vivo* glioblastoma distribution of NPs was studied qualitatively by fluorescence microscopic observation of tumor tissues. Results showed that strong green fluorescence signals from the tumor slices of targeting group, indicating the much more significant uptake of ANG/PEG-UCNPs than that of PEG-UCNPs by glioblastoma cells (Figure S14). Moreover, the concentration of Y element in brain was quantitatively measured by ICP-OES after the intravenous injection with ANG/PEG-UCNPs for 1 h. As shown in Figure S15, the amount of ANG/PEG-UCNPs uptake by glioblastoma was 3.6-fold higher than that of PEG-UCNPs, confirming the significant tumor targeting capability of ANG/PEG-UCNPs. Compared to the low uptake in the normal brain tissue, the significant uptake of ANG/PEG-UCNPs in the tumor illustrates that these dual-targeting NPs could cross the BBB and then accumulated in tumor regions by specifically linking to LRP receptors overexpressed on both BBB and glioblastoma, which is well consistent with the above imaging observations.

Toxicity Studies. Although various nanomaterials have been reported for crossing the BBB, little attention has been paid for the materials' biocompatibility which is vital for their further application *in vivo*. As the deposition of

these nanomaterials in the brain may have negative influence on the brain, and lead to the potential toxicity,[15−17] the toxicity of BBB-crossing NPs needs to be assessed urgently. Here, *in vivo* toxicity of ANG/PEG-UCNPs has been investigated by body weight measurements, hematoxylin and eosin (H&E) staining analysis, blood biochemistry and hematology tests. Undulation in body weight is a direct indicator for the ANG/PEG-UCNPs toxicity effect *in vivo*. The body weights of the mice injected with or without the NPs were recorded for one month and the results are shown in Figure S16. There is no difference in body weights between the test group and the control group, indicating that ANG/PEG-UCNPs had no overall side effect on the investigated mice.

To evaluate the brain toxicity of ANG/PEG-UCNPs, the tissue sections of cortex, hippocampus and striatum collected after single intravenous injection of ANG/PEG-UCNPs for 3, 15, and 30 days were stained with H&E. As presented in Figure 6a, there is no visible tissue damage or any other side effect to cortex, hippocampus and striatum as compared with the control group, which verifies that no visible lesions take place in the brain after the ANG/PEG-UCNPs treatment. In the meantime, no side effects were observed on heart, liver, spleen, lung and kidney (Figure S17), exhibiting the good biocompatibility of ANG/PEG-UCNPs. Furthermore, we performed the serum biochemistry and hematology analyses to investigate the influence of ANG/PEG-UCNPs on the healthy mice quantitatively. Figure 6b shows that no obvious hepatic toxicity has been induced by the NPs treatment, as indicated by normal values of the liver function markers including ALT, AST and AKP. As indicators of kidney functions, the CRE and BUN levels in the blood of treated mice are also normal, demonstrating little side effect of these NPs on kidney (Figure 6c,d). For the hematology analysis, the blood parameters in the treatment groups over time appeared to be normal compared with the control groups (Figure 6e−m). In a word, the above results offer a preliminary validation that ANG/PEG-UCNPs bear no significant appreciable toxicity *in vivo* and therefore are promising medical imaging contrast agents.

CONCLUSIONS

In summary, a novel BBB and glioblastoma dual-targeted brain nanoprobe has been successfully constructed by covalently coupling Angiopep-2 with the PEG-coated UCNPs. Both cellular and animal experimental results demonstrate that the ANG/PEG-UCNPs nanoprobes can cross the BBB by receptor-mediated transcytosis and subsequently target glioblastoma efficiently. Moreover, the ANG/PEG-UCNPs bimodal nanoprobes show a great potential in preoperative diagnosing and intraoperative positioning the brain tumors by MR and NIR-to-NIR UCL fluorescence imaging, exhibiting the more excellent imaging performances as compared to the clinically used MRI contrast Gd-DTPA and fluorescent dye 5-ALA. Meanwhile, no apparent *in vivo* side effects have been observed in toxicity studies, exhibiting good biocompatibility. Noticeably, high *Z*-value based UCNPs have been demonstrated to be effective radiosensitizers for tumor radiotherapy in our previous report.[43] Therefore, we anticipate that the present ANG/PEG-UCNPs will also be highly attractive to enhance the overall effectiveness of brain tumor therapy with radiotherapy.

METHODS

Materials. $YCl_3 \cdot 6H_2O$, $YbCl_3 \cdot 6H_2O$, $TmCl_3$, $GdCl_3 \cdot 6H_2O$, ammonium fluoride (NH_4F), 1-octacene (90%), 1-(3-dimethylaminopropyl)-3-ethylcarbodiimide hydrochloride (EDC), *N*-hydroxysuccinimide (NHS) and 5-aminolevulinic acid (5-ALA) were purchased from Sigma-Aldrich. Oleic acid (OA) and methanol (CH_3OH) were obtained from Shanghai Lingfeng Chemical Reagent Co., Ltd. Sodium hydroxide (NaOH) and hydrochloric acid (HCl, 36−38%) were acquired from Sinopharm Chemical Reagent Co., Ltd. NH_2-PEG_{5k}-SH and MeO-PEG_{5k}-SH were obtained from Jenkem Co., Ltd. Angiopep-2 (TFFYGGSRGKRNNFKTEEY) was purchased from Chinese Peptide Company. Magnevist (Gd-DTPA) was provided by Huashan Hospital. All reagents were of analytical grade and used without any purification.

Cytotoxicity Assessment. Human glioblastoma cells U87MG were cultured at 37 °C and with 5% CO_2 in Dulbecco's Modified Eagle Medium (DMEM) supplemented with 10% fetal bovine serum (FBS) and 1% penicillin/streptomycin. Brain capillary endothelial cells (BCECs) were cultured at 37 °C and with 5% CO_2 in Roswell Park Memorial Institute medium (RPMI) 1640 supplemented with 15% fetal bovineserum (FBS) and 1% penicillin/streptomycin. The cell cytotoxicity *in vitro* was measured by 3-(4, 5-dimethylthiazol-2-yl)-2, 5-diphenyltetrazolium bromide (MTT) assay. Cells were seeded into a 96-well cell culture plate at 10^6/well and then incubated for 24 h at 37 °C under 5% CO_2. RPMI 1640/DMEM solutions of ANG/PEG-UCNPs or PEG-UCNPs with different concentrations of 7.81, 15.62, 31.25, 62.5, 125, 250, 500, and 1000 μg/mL were added to the wells. The cells were then incubated for 24 h at 37 °C under 5% CO_2; the cell viability was calculated using a typical MTT assy.

Enhanced Cellular Uptake *in Vitro*. U87MG and BCECs were seeded at a density of 10^5 cells/well in a CLSM-special cell culture dish and incubated for 24 h at 37 °C under 5% CO_2. The ANG/PEG-UCNPs and PEG-UCNPs were dispersed into RPMI 1640/DMEM cell-culture media with a concentration of 300 μg/mL, and then added into the culture dish. One hour after co-incubation, the cells were washed three times with PBS to remove the nonuptake nanoparticles followed by nuclei staining by DAPI. Then confocal fluorescence imaging experiments were performed on an Olympus FV1000 laser-scanning microscope equipped with a CW NIR laser (λ = 980 nm), while DAPI was excited with 358 nm light. A 60× oil immersion objective lens was used and luminescence signals were detected in the wavelength regions of 400−500 nm. To provide further evidence of ANG-mediated transcytosis mechanism, a blocking study was carried out by adding ANG to the wells in advance at a concentration of 3 mg/mL. The compounds were withdrew from the wells 0.5 h after incubation at 37 °C under 5% CO_2, and 300 μg/mL ANG/PEG-UCNPs, along with ANG at a concentration of 3 mg/mL, was added and incubated for 1 h, followed by above-mentioned steps.

Transport across the BBB Model *in Vitro*. For the construction of the BBB *in vitro* model, which was used to study the BBB permeability of nanoparticles by Fang *et al.*,[45] BCECs, at a

density of 5×10^4 cells/well, were seeded on polycarbonate 24-well transwell membranes of 1.0 μm mean pore size, 0.33 cm^2 surface areas (FALCON Cell Culture Insert, Becton Dickinson Labware, USA). After 4 days, the cell monolayer integrity was monitored using an epithelial voltohmmeter (Millicell-RES, Millipore, USA), and the cells with Transendothelial Electrical Resistance (TEER) values above 200 $\Omega \cdot cm^2$ were selected for the transfer experiments. ANG/PEG-UCNPs (Gd 10 μg/mL), diluted in RPMI 1640, was introduced into the apical side chamber (blood side *in vivo*) of the BBB model, shaking at 50 rpm at 37 °C. The TEER values were measured during the incubation. The basolateral medium and the filter membrane with the cells separated from the support were collected 18 h after incubation, for measuring the Gd content by inductively coupled plasma optical emission spectrometry (ICP-OES). In parallel, the same procedures were also applied for the control experiments based on the PEG-UCNPs with the same concentrations. To provide future evidence for the ANG-mediated transcytosis mechanism, a blocking study was carried out by adding ANG to the apical side chamber in advanced at a concentration of 3 mg/mL. The compounds were withdrawn from the transwell 0.5 h after incubation at 37 °C, and ANG/PEG-UCNPs (Gd 10 μg/mL), along with ANG at concentration 3 mg/mL, was added, followed by above-mentioned steps.

Transport across the BBB *in Vivo* and MRI of Intracranial Glioblastoma. All animal experiments were in agreement with the guidelines of the Institutional Animal Care and Use Committee. Male Balb/c nude mice with average weight of 20 g were purchased from laboratory animal center; Shanghai Medical College of Fudan University. *In vivo* MRI was carried out on a 3.0-T clinical MRI instrument (Siemens Magnetom Trio Tim 3.0T MRI). T_1-weighted MR images of the brain sections were acquired with the turbo spin echo (TSE) sequence: TR = 529 ms; TE = 14 ms; TD = 0.0 ms; Slice thickness = 1.5 mm; Field of view (Fov) read = 60 mm; Fov phase = 75%; matrix = 384 × 384; Flip angle = 120 °C; Fat suppress, None; Water Suppress, None. T_2-weighted MR images of the brain sections were acquired with the turbo spin echo (TSE) sequence: TR = 2500 ms; TE = 76 ms; slice thickness = 1.5 mm; Field of view (Fov) read = 60 mm; Fov phase = 59.9%; matrix = 384 × 384; Flip angle = 117 °C; Fat suppress, None; Water Suppress, None.

To investigate the ANG-mediated transport of UCNPs across the BBB *in vivo*, T_1-weighted MR images of normal mice brain were collected before and 1 h after administration of Gd-DTPA or ANG/PEG-UCNPs with a dose of 150 μL (6 mg Gd/kg dose, $n = 3$) *via* intravenous injection. The regions of interest (ROI) at the same position and with the same circular area located in the right brain parenchyma of the healthy brain were marked on MR images before and after injection. And the signal intensity of ROI in the brain was then measured.

To compare the targeted ANG/PEG-UCNPs effect for U87MG *in vivo*, the intracranial glioblastoma-bearing mice model were established as reported.[16] Briefly, U87MG cells (5×10^5 suspended in 5 μL PBS) were implanted into the striatum (1.8 mm lateral and 3 mm of depth) of male Balb/c nude mice by using a stereotactic fixation device with mouse adapter. The intracranial glioblastoma-bearing mice were ready for imaging after inoculation for 14−18 days. T_1-weighted MR images of glioblastoma-bearing mice brain were collected before and 10 min, 0.5, 1, 2, 8, 24, 48 h after administration of ANG/PEG-UCNPs, PEG-UCNPs or Gd-DTPA with a dose of 150 μL (6 mg Gd/kg dose) *via* intravenous injection. And tumor regions of interest (ROI) with the same circular area were carefully selected on T_1-weighted MR images before and after injection according to the previous T_2-weighted images' delineation. And the signal intensity of ROI in the brain tumor was then measured.

NIR-to-NIR Fluorescence Imaging of Intracranial Glioblastoma *ex Vivo*. *Ex vivo* NIR-to-NIR UCL imaging was carried out by using a homemade UCL *in vivo* imaging system from Prof. Li's group (Advanced Materials Laboratory, Department of Chemistry, Fudan University). Excitation was provided by using an external 0−5 W adjustable CW infrared laser (980 nm, Shanghai Connet Fiber Optics, China). UCL signals were collected at 800 ± 12 nm and images of UCL signals were analyzed with Kodak Molecular Imaging Software. The tumor-bearing brain was then removed for *ex vivo* imaging in 1 h after the intravenous injection with ANG/PEG-UCNPs and PEG-UCNPs at a total dose of 150 μL (15 mg Y/kg dose). The clinical 5-ALA was used for comparison experiment at a total dose of 150 μL (90 mg/kg dose). Then *ex vivo* fluorescence imaging of glioblastoma-bearing brain were conducted on imaging machine (Bruker, excitation, 470 nm; emission, 650 nm.) in 1 h after the postinjection. All imaging experiments were performed under the same condition. After completion of fluorescence imaging, the mice brain were frozen, and H&E-stained tumor sections from mice brain were used to further ensure the existence of brain tumor. The histological sections were observed under optical microscope.

Toxicity Studies *in Vivo*. Kunming mice with average weight of 20 g were purchased from laboratory animal center; shanghai medical college of Fudan University. The ANG/PEG-UCNPs at a total dose of 150 μL (15 mg Y/kg dose) were injected into Kunming mice ($n = 5$) *via* the intravenous injection and this group of mice was used as the experimental group. Kunming mice ($n = 5$) with no injection of the ANG/PEG-UCNPs were selected as the control group. The body weights of the mice in both groups were recorded for 30 days. Blood samples and tissues were harvested from mice in control group or mice injected with ANG/PEG-UCNPs on 3, 15, and 30 days postinjection. Three important hepatic indicators (alanine aminotransferase (ALT), aspartate aminotransferase (AST) and Alkaline phosphatase (AKP)), and two indicators for kidney functions (creatinine (CRE) and blood urea nitrogen (BUN)) were measured. The complete blood panel data from healthy control and treated mice (white blood cells, red blood cells, mean corpuscular hemoglobin, mean corpuscular hemoglobin concentration, and mean corpuscular volume, hemoglobin, red cell distribution width, hematocrit and lymphocyte) were tested. After completion of the blood collection, the mice were sacrificed. H&E-stained tissue sections from mice to monitor the histological changes in brain (cortex, hippocampus and striatum), liver, spleen, heart, lung and kidney of mice were collected. The histological sections were observed under an optical microscope.

Characterization. Transmission electron microscopy (TEM) images and energy-dispersive X-ray analysis (EDXA) were performed on a JEOL 200CX microscope with an accelerating voltage of 200 kV. Powder X-ray diffraction patterns were performed on a Rigaku D/MAX-2250 V diffract meter with graphite-monochromatized Cu Kα radiation. Fourier transform infrared spectroscopy (FT-IR) spectra were recorded on a Nicolet Avatar 370 FT-IR spectrophotometer using KBr pellets. Dynamic light scattering (DLS) measurement was conducted on Nano-Zetesizer (Malvern Instruments Ltd.). The Y, Gd concentrations of samples were measured by inductively coupled plasma optical emission spectrometry (ICP-OES). Upconversion luminescence emission spectra were collected on Fluorolog-3 Spectrofluorometer (Jobin Yvon, France) with the excitation of a 450W xenon lamp and an external 0−1 W adjustable 980 nm semiconductor laser (Beijing Hi-tech Optoelectronic Co., China). CLSM images were recorded on FV 1000, Olympus, Japan.

Conflict of Interest: The authors declare no competing financial interest.

Acknowledgment. This work has been financially supported by the National Natural Science Foundation of China (Grant No. 51372260, 51132009, 21172043, 51072212, 51102259, 81271633), the Shanghai Rising-Star Program (Grant No. 12QH1402500), the Nano special program of the Science and Technology Commission of Shanghai (Grant No.11 nm0505000), the Development Foundation for Talents of Shanghai (Grant No.2012035), Opening Project of State Key Laboratory of High Performance Ceramics and Superfine Microstructure (Grant No. SKL201303SIC). We thank Prof. Fuyou Li, Dr. Yang Yang and Xingjun Zhu from Fudan University for the help in UCL *ex vivo* imaging. We thank Prof. Wei Hua from Huashan Hospital for the help in building the intracranial glioblastoma-bearing mice model. We thank Yu Chen, Chen Zhang, Yanyan Liu, Jingwei Feng, Zheng Wang, Haiyun Qu, Linlin Zhang and Heliang Yao from Shanghai Institute of Ceramics, Chinese Academy of Sciences for useful discussions.

Supporting Information Available: Synthetic procedures for UCNPs, OA-free UCNPs, PEG-UCNPs, ANG/PEG-UCNPs, and other supplementary figures. This material is available free of charge *via* the Internet at http://pubs.acs.org.

REFERENCES AND NOTES

1. Huse, J. T.; Holland, E. C. Targeting Brain Cancer: Advances in the Molecular Pathology of Malignant Glioma and Medulloblastoma. *Nat. Rev. Cancer* **2010**, *10*, 319–331.
2. Wen, P. Y.; Kesari, S. Malignant Gliomas in Adults. *Engl. J. Med.* **2008**, *359*, 492–507.
3. Krex, D.; Klink, B.; Hartmann, C.; von Deimling, A.; Pietsch, T.; Simon, M.; Sabel, M.; Steinbach, J. P.; Heese, O.; Reifenberger, G.; *et al.* Long-Term Survival With Glioblastoma Multiforme. *Brain* **2007**, *130*, 2596–2606.
4. Donahue, M. J.; Blakeley, J. O.; Zhou, J. Y.; Pomper, M. G.; Laterra, J.; van Zijl, P. C. M. Evaluation of Human Brain Tumor Heterogeneity Using Multiple T_1-Based MRI Signal Weighting Approaches. *Magn. Reson. Med.* **2008**, *59*, 336–344.
5. Kircher, M. F.; de la Zerda, A.; Jokerst, J. V.; Zavaleta, C. L.; Kempen, P. J.; Mittra, E.; Pitter, K.; Huang, R.; Campos, C.; Habte, F.; Sinclair, R.; *et al.* A brain Tumor Molecular Imaging Strategy Using a New Triple-Modality MRI-Photoacoustic-Raman Nanoparticle. *Nat. Med.* **2012**, *18*, 829–834.
6. Yang, I.; Aghi, M. K. New Advances That Enable Identification of Glioblastoma Recurrence. *Nat. Rev. Clin. Oncol.* **2009**, *6*, 648–657.
7. Zhou, J. Y.; Tryggestad, E.; Wen, Z. B.; Lal, B.; Zhou, T. T.; Grossman, R.; Wang, S. L.; Yan, K.; Fu, D. X.; Ford, E.; *et al.* Differentiation Between Glioma and Radiation Necrosis Using Molecular Magnetic Resonance Imaging of Endogenous Proteins and Peptides. *Nat. Med.* **2011**, *17*, 130–134.
8. Giesel, F. L.; Mehndiratta, A.; Essig, M. High-Relaxivity Contrast-Enhanced Magnetic Resonance Neuroimaging: a review. *Eur. Radiol.* **2010**, *20*, 2461–2474.
9. Kievit, F. M.; Zhang, M. Q. Cancer Nanotheranostics: Improving Imaging and Therapy by Targeted Delivery across Biological Barriers. *Adv. Mater.* **2011**, *23*, H217–H247.
10. Orive, G.; Ali, O. A.; Anitua, E.; Pedraz, J. L.; Emerich, D. F. Biomaterial-Based Technologies for Brain Anti-Cancer Therapeutics and Imaging. *Biochim. Biophys. Acta, Rev. Cancer* **2010**, *1806*, 96–107.
11. Veiseh, O.; Sun, C.; Fang, C.; Bhattarai, N.; Gunn, J.; Kievit, F.; Du, K.; Pullar, B.; Lee, D.; Ellenbogen, R. G.; *et al.* Specific Targeting of Brain Tumors with an Optical/Magnetic Resonance Imaging Nanoprobe across the Blood-Brain Barrier. *Cancer Res.* **2009**, *69*, 6200–6207.
12. Scott, J. N.; Brasher, P. M. A.; Sevick, R. J.; Rewcastle, N. B.; Forsyth, P. A. How Often Are Nonenhancing Supratentorial Gliomas Malignant? A population Study. *Neurology* **2002**, *59*, 947–949.
13. Caravan, P.; Ellison, J. J.; McMurry, T. J.; Lauffer, R. B. Gadolinium(III) Chelates as MRI Contrast Agents: Structure, Dynamics, and Applications. *Chem. Rev.* **1999**, *99*, 2293–2352.
14. Lee, D. E.; Koo, H.; Sun, I. C.; Ryu, J. H.; Kim, K.; Kwon, I. C. Multifunctional Nanoparticles for Multimodal Imaging and Theragnosis. *Chem. Soc. Rev.* **2012**, *41*, 2656–2672.
15. Qiao, R. R.; Jia, Q. J.; Huwel, S.; Xia, R.; Liu, T.; Gao, F. B.; Galla, H. J.; Gao, M. Y. Receptor-Mediated Delivery of Magnetic Nanoparticles across the Blood-Brain Barrier. *ACS Nano* **2012**, *6*, 3304–3310.
16. Yan, H. H.; Wang, L.; Wang, J.; Weng, X. F.; Lei, H.; Wang, X. X.; Jiang, L.; Zhu, J. H.; Lu, W. Y.; Wei, X. B.; *et al.* Two-Order Targeted Brain Tumor Imaging by Using an Optical/Paramagnetic Nanoprobe across the Blood Brain Barrier. *ACS Nano* **2012**, *6*, 410–420.
17. Georgieva, J. V.; Brinkhuis, R. P.; Stojanov, K.; Weijers, C. A.; Zuilhof, H.; Rutjes, F. P.; Hoekstra, D.; van Hest, J. C.; Zuhorn, I. S. Peptide-Mediated Blood-Brain Barrier Transport of Polymersomes. *Angew. Chem., Int. Ed.* **2012**, *51*, 8339–8342.
18. Lu, W.; Sun, Q.; Wan, J.; She, Z. Y.; Jiang, X. G. Cationic Albumin-Conjugated Pegylated Nanoparticles Allow Gene Delivery into Brain Tumors *via* Intravenous Administration. *Cancer Res.* **2006**, *66*, 11878–11887.
19. Yim, Y. S.; Choi, J. S.; Kim, G. T.; Kim, C. H.; Shin, T. H.; Kim, D. G.; Cheon, J. A Facile Approach for the Delivery of Inorganic Nanoparticles into the Brain by passing through the Blood-Brain Barrier (BBB). *Chem. Commun.* **2012**, *48*, 61–63.
20. He, H.; Li, Y.; Jia, X. R.; Du, J.; Ying, X.; Lu, W. L.; Lou, J. N.; Wei, Y. PEGylated Poly(amidoamine) Dendrimer-Based Dual-Targeting Carrier for Treating Brain Tumors. *Biomaterials* **2011**, *32*, 478–487.
21. Stummer, W.; Pichlmeier, U.; Meinel, T.; Wiestler, O. D.; Zanella, F.; Reulen, H. J. Fluorescence-Guided Surgery with 5-Aminolevulinic Acid for Resection of Malignant Glioma: a Randomised Controlled Multicentre Phase III Trial. *Lancet Oncol.* **2006**, *7*, 392–401.
22. Kircher, M. F.; Mahmood, U.; King, R. S.; Weissleder, R.; Josephson, L. A Multimodal Nanoparticle for Preoperative Magnetic Resonance Imaging and Intraoperative Optical Brain Tumor Delineation. *Cancer Res.* **2003**, *63*, 8122–8125.
23. Santra, S.; Yang, H.; Stanley, J. T.; Holloway, P. H.; Moudgil, B. M.; Walter, G.; Mericle, R. A. Rapid and Effective Labeling of Brain Tissue Using TAT-Conjugated CdS:Mn/ZnS Quantum Dots. *Chem. Commun.* **2005**, 3144–3146.
24. Li, L. H.; Guo, K.; Lu, J.; Venkatraman, S. S.; Luo, D.; Ng, K. C.; Ling, E. A.; Moochhala, S.; Yang, Y. Y. Biologically Active Core/Shell Nanoparticles Self-Assembled from Cholesterol-Terminated PEG-TAT for Drug Delivery across the Blood-Brain Barrier. *Biomaterials* **2008**, *29*, 1509–1517.
25. Nabavi, A.; Thurm, H.; Zountsas, B.; Pietsch, T.; Lanfermann, H.; Pichlmeier, U.; Mehdorn, M. Five-Aminolevulinic Acid for Fluorescence-Guided Resection of Recurrent Malignant Gliomas: A Phase II Study. *Neurosurgery* **2009**, *65*, 1070–1076.
26. Tonn, J. C.; Stummer, W. Fluorescence-Guided Resection of Malignant Gliomas Using 5-aminolevulinic Acid:Practical Use, Risks, and Pitfalls. *Clin. Neurosurg.* **2008**, *55*, 20–26.
27. Wang, F.; Liu, X. G. Recent Advances in the Chemistry of Lanthanide-Doped Upconversion Nanocrystals. *Chem. Soc. Rev.* **2009**, *38*, 976–989.
28. Liu, Y. S; Tu, D. T; Zhu, H. M; Chen, X. Y. Lanthanide-Doped Luminescent Nanoprobes: Controlled Synthesis, Optical Spectroscopy, and Bbioapplications. *Chem. Soc. Rev.* **2013**, *42*, 6924–6958.
29. Gu, Z. J.; Yan, L.; Tian, G.; Li, S. J.; Chai, Z. F.; Zhao, Y. L. Recent Advances in Design and Fabrication of Upconversion Nanoparticles and Their Safe Theranostic Applications. *Adv. Mater.* **2013**, *25*, 3758–3779.
30. Liu, Q.; Sun, Y.; Yang, T. S.; Feng, W.; Li, C. G.; Li, F. Y. Sub-10 nm Hexagonal Lanthanide-Doped $NaLuF_4$ Upconversion Nanocrystals for Sensitive Bioimaging *in Vivo*. *J. Am. Chem. Soc.* **2011**, *133*, 17122–17125.
31. Cheng, L.; Yang, K.; Li, Y. G.; Chen, J. H.; Wang, C.; Shao, M. W.; Lee, S. T.; Liu, Z. Facile Preparation of Multifunctional Upconversion Nanoprobes for Multimodal Imaging and Dual-Targeted Photothermal Therapy. *Angew. Chem., Int. Ed.* **2011**, *50*, 7385–7390.
32. Gai, S. L.; Yang, P. P.; Li, C. X.; Wang, W. X.; Dai, Y. L.; Niu, N.; Lin, J. Synthesis of Magnetic, Up-Conversion Luminescent, and Mesoporous Core-Shell-Structured Nanocomposites as Drug Carriers. *Adv. Funct. Mater.* **2010**, *20*, 1166–1172.
33. Zhou, J. C.; Yang, Z. L.; Dong, W.; Tang, R. J.; Sun, L. D.; Yan, C. H. Bioimaging and Toxicity Assessments of Near-Infrared Upconversion Luminescent $NaYF_4$:Yb,Tm Nanocrystals. *Biomaterials* **2011**, *32*, 9059–9067.
34. Idris, N. M.; Gnanasammandhan, M. K.; Zhang, J.; Ho, P. C.; Mahendran, R.; Zhang, Y. *In vivo* Photodynamic Therapy Using Upconversion Nanoparticles as Remote-Controlled Nanotransducers. *Nat. Med.* **2012**, *18*, 1580–1585.
35. Yang, T. S.; Sun, Y.; Liu, Q.; Feng, W.; Yang, P. Y.; Li, F. Y. Cubic Sub-20 nm $NaLuF_4$-Based Upconversion Nanophosphors for High-Contrast Bioimaging in Different Animal Species. *Biomaterials* **2012**, *33*, 3733–3742.
36. Park, Y. I.; Kim, J. H.; Lee, K. T.; Jeon, K. S.; Na, H. B.; Yu, J. H.; Kim, H. M.; Lee, N.; Choi, S. H.; Baik, S. I.; *et al.* Nonblinking

and Nonbleaching Upconverting Nanoparticles as an Optical Imaging Nanoprobe and T_1 Magnetic Resonance Imaging Contrast Agent. *Adv. Mater.* **2009**, *21*, 4467–4471.
37. Park, Y. I.; Kim, H. M.; Kim, J. H.; Moon, K. C.; Yoo, B.; Lee, K. T.; Lee, N.; Choi, Y.; Park, W.; Ling, D. S.; Na, K.; *et al.* Theranostic Probe Based on Lanthanide-Doped Nanoparticles for Simultaneous *in Vivo* Dual-Modal Imaging and Photodynamic Therapy. *Adv. Mater.* **2012**, *24*, 5755–5761.
38. Abel, K. A.; Boyer, J. C.; van Veggel, F. C. Hard Proof of the $NaYF_4$/$NaGdF_4$ Nanocrystal Core/Shell Structure. *J. Am. Chem. Soc.* **2009**, *131*, 14644–14645.
39. Kumar, R.; Nyk, M.; Ohulchanskyy, T. Y.; Flask, C. A.; Prasad, P. N. Combined Optical and MR Bioimaging Using Rare Earth Ion Doped $NaYF_4$ Nanocrystals. *Adv. Funct. Mater.* **2009**, *19*, 853–859.
40. Chen, F.; Bu, W. B.; Zhang, S. J.; Liu, J. N.; Fan, W. P.; Zhou, L. P.; Peng, W. J.; Shi, J. L. Gd^{3+}-Ion-Doped Upconversion Nanoprobes: Relaxivity Mechanism Probing and Sensitivity Optimization. *Adv. Funct. Mater.* **2013**, *23*, 298–307.
41. Chen, F.; Bu, W. B.; Zhang, S.; Liu, X. H.; Liu, J. N.; Xing, H. Y.; Xiao, Q. F.; Zhou, L. P.; Peng, W. J.; Wang, L. Z.; *et al.* Positive and Negative Lattice Shielding Effects Co-existing in Gd (III) Ion Doped Bifunctional Upconversion Nanoprobes. *Adv. Funct. Mater.* **2011**, *21*, 4285–4294.
42. Jin, J.; Xu, Z.; Zhang, Y.; Gu, Y. J.; Lam, M. H.; Wong, W. T. Upconversion Nanoparticles Conjugated with Gd -DOTA and RGD for Targeted Dual-Modality Imaging of Brain Tumor Xenografts. *Adv. Healthcare Mater.* **2013**, *2*, 1501–1512.
43. Xing, H. Y.; Zheng, X. P.; Ren, Q. G.; Bu, W. B.; Ge, W. Q.; Xiao, Q. F.; Zhang, S. J.; Wei, C. Y.; Qu, H. Y.; Wang, Z.; *et al.* Computed Tomography Imaging-Guided Radiotherapy by Targeting Upconversion Nanocubes with Significant Imaging and Radiosensitization Enhancements. *Sci. Rep.* **2013**, *3*, 1571(1)–1571(9).
44. Sun, X. Y.; Pang, Z. Q.; Ye, H. X.; Qiu, B.; Guo, L. R.; Li, J. W.; Ren, J. F.; Qian, Y.; Zhang, Q. Z.; Chen, J.; *et al.* Co-delivery of pEGFP-hTRAIL and Paclitaxel to Brain Glioma Mediated by an Angiopep-Conjugated Liposome. *Biomaterials* **2012**, *33*, 916–924.
45. Xin, H. L.; Jiang, X. Y.; Gu, J. J.; Sha, X. Y.; Chen, L. C.; Law, K.; Chen, Y. Z.; Wang, X.; Jiang, Y.; Fang, X. L. Angiopep-Conjugated Poly(ethylene glycol)-Co-Poly(ε-caprolactone) Nanoparticles as Dual-Targeting Drug Delivery System for Brain Glioma. *Biomaterials* **2011**, *32*, 4293–4305.
46. Huang, S. X.; Li, J. F.; Han, L.; Liu, S. H.; Ma, H. J.; Huang, R. Q.; Jiang, C. Dual Targeting Effect of Angiopep-2-Modified, DNA-Loaded Nanoparticles for Glioma. *Biomaterials* **2011**, *32*, 6832–6838.
47. Fan, W. P.; Shen, B.; Bu, W. B.; Chen, F.; Zhao, K. L.; Zhang, S. J.; Zhou, L. P.; Peng, W. J.; Xiao, Q. F.; Xing, H. Y.; *et al.* Rattle-Structured Multifunctional Nanotheranostics for Synergetic Chemo-/Radiotherapy and Simultaneous Magnetic/Luminescent Dual-Mode Imaging. *J. Am. Chem. Soc.* **2013**, *135*, 6494–6503.
48. Bogdan, N.; Vetrone, F.; Ozin, G. A.; Capobianco, J. A. Synthesis of Ligand-Free Colloidally Stable Water Dispersible Brightly Luminescent Lanthanide-Doped Upconverting Nanoparticles. *Nano Lett.* **2011**, *11*, 835–840.
49. Lu, Z. D.; Gao, C. B.; Zhang, Q.; Chi, M. F.; Howe, J. Y.; Yin, Y. D. Direct Assembly of Hydrophobic Nanoparticles to Multifunctional Structures. *Nano Lett.* **2011**, *11*, 3404–3412.
50. Liu, J. N.; Bu, W. B.; Pan, L. M.; Zhang, S. J.; Chen, F.; Zhou, L. P.; Zhao, K. L.; Peng, W. J.; Shi, J. L. Simultaneous Nuclear Imaging and Intranuclear Drug Delivery by Nuclear-targeted Multifunctional Upconversion Nanoprobes. *Biomaterials* **2012**, *33*, 7282–7890.
51. Xiao, Q. F.; Bu, W. B.; Ren, Q. G.; Zhang, S. J.; Xing, H. Y.; Chen, F.; Li, M.; Zheng, X. P.; Hua, Y. Q.; Zhou, L. P.; *et al.* Radiopaque Fluorescence-Transparent TaO(x) Decorated Upconversion Nanophosphors for *in vivo* CT/MR/UCL Trimodal Imaging. *Biomaterials* **2012**, *33*, 7530–7539.
52. Vuong, Q. L.; Van Doorslaer, S.; Bridot, J. L.; Argante, C.; Alejandro, G.; Hermann, R.; Disch, S.; Mattea, C.; Stapf, S.; Gossuin, Y. Paramagnetic Nanoparticles as Potential MRI Contrast Agents: Characterization, NMR Relaxation, Simulations and Theory. *Magn. Reson. Mater. Phys.* **2012**, *25*, 467–578.
53. Naccache, R.; Chevallier, P.; Lagueux, J.; Gossuin, Y.; Laurent, S.; Vander Elst, L.; Chilian, C.; Capobianco, J. A.; Fortin, M. A. High Relaxivities and Strong Vascular Signal Enhancement for $NaGdF_4$ Nanoparticles Designed for Dual MR/Optical Imaging. *Adv. Healthcare Mater.* **2013**, *2*, 1477–1488.
54. Kramer, K. W.; Biner, D.; Frei, G.; Gudel, H. U.; Hehlen, M. P.; Luthi, S. R. Hexagonal Sodium Yttrium Fluoride Based Green and Blue Emitting Upconversion Phosphors. *Chem. Mater.* **2004**, *16*, 1244–1251.
55. Wang, F.; Han, Y.; Lim, C. S.; Lu, Y. H.; Wang, J.; Xu, J.; Chen, H. Y.; Hong, M. H.; Liu, X. G. Simultaneous Phase and Size Control of Upconversion Nanocrystals Through Lanthanide Doping. *Nature* **2010**, *463*, 1061–1065.